Contrib Mineral Petrol (1996) 122:359–367

Jibamitra Ganguly · M. Chiara Domeneghetti

Cation ordering of orthopyroxenes from the Skaergaard Intrusion: implications for the subsolidus cooling rates and permeabilities

Received: 27 February 1995/Accepted: 20 July 1995

Abstract We have determined the quenched cation ordering states of five orthopyroxene crystals collected from the marginal border group and the lower zone a and b of the Skaergaard intrusion, and modeled these data to retrieve their closure temperatures (T_c) of Fe–Mg ordering and cooling rates. According to existing thermal models for the Skaergaard pluton, conductive cooling dominated the high and low temperature regimes, which were separated by an intermediate temperature regime in which the cooling was controlled primarily by convective fluid circulation. The cooling rates retrieved from the quenched cation ordering states of the orthopyroxene crystals strictly apply to temperatures around the closure temperatures of the ordering states, ~ 340–400° C, which fall at the transition from convective to the lower temperature conductive cooling. The cooling rates obtained from the cation ordering states of orthopyroxene vary from ~ 1 to 270 K/ka. These results agree well with a thermal model calculated using an assumed average permeability of 10^{-12} cm^2 for the pluton, but not completely with a model calculated on the basis of an average permeability of 10^{-13} cm^2, although both values produced shifts of δ^{18}O that are comparable to those observed in the pluton.

Introduction

Since its discovery and initial studies by Wager and Deer (1939), the gabbroic intrusion in Skaergaard, East Greenland, has attracted the attention of generations of petrologists, mineralogists and geochemists. Observational data extracted from this intrusive body have fundamentally influenced our understanding of the crystallization-differentiation processes in magmas (e.g., Wager and Brown 1968). In a seminal study of transport processes in magma-hydrothermal systems, Norton and Taylor (1979) developed detailed numerical models of interaction between the crystallizing Skaergaard pluton and the circulating fluid using the measured shifts of δ^{18}O values in the pluton as constraints. These fluid-rock interaction models also yield quantitative cooling history models of the pluton in both conduction and fluid convection dominated regimes. The purpose of the present paper is to retrieve cooling rates from the quenched cation ordering properties of orthopyroxenes (e.g., Ganguly 1982; Ganguly et al. 1994) in selected locations of the intrusive body. The results would provide a test of the numerical models of Norton and Taylor (1979) and lead to additional constraints on the permeability values of the intrusive body.

The orthopyroxene samples were separated from rocks collected during several expeditions to Skaergaard and kindly donated to us by Dennis Bird, Alexander McBirney, Stewart McCallum, and Denis Norton. The primary sample numbers and their locations are as follows. *IVN-14*: marginal border group (MBG) in Invarmuit Island ~ 30 m from the contact of upper zone a; *CG-372*, *CG-379* lower zone a, ~ 150 and 550 m from the contact with MBG, respectively; *CG-380* and *SK90-5* base of lower zone b, very close to the contact with the lower zone a. Locations of all samples excepting IVN-14 are illustrated in Fig. 1a. The last sample was collected from MBG approximately 6 km S15 W of its termination in the map area illustrated in Fig. 1a. A simplified east-west cross sectional view of the pluton, adapted from McBirney (1993), is illustrated in Fig. 1b. For extended plan view and further discussions about the nature of the pluton, interested

J. Ganguly (✉)
Department of Geosciences, University of Arizona
Tucson, AZ 85721, USA

M. C. Domeneghetti
CNR-Centro di Studio per la Cristallochimica e la Cristallografia,
Dipartimento di Scienze della Terra, Università di Pavia,
Via Abbiategrasso 209, I-27100 Pavia, Italy

Editorial responsibility: T. L. Grove

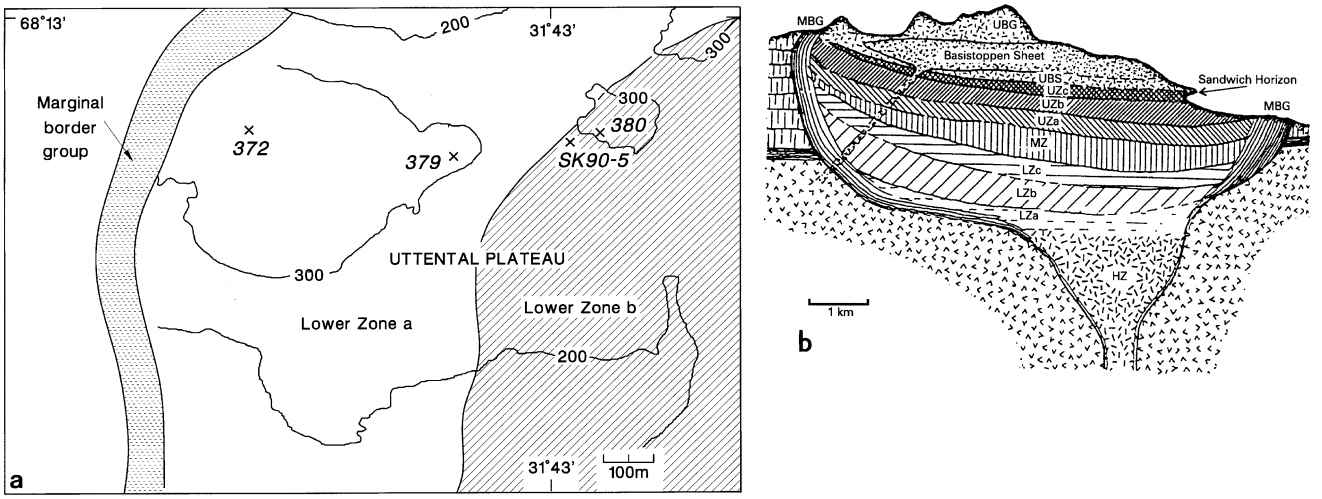

Fig. 1a Location map of the samples from the Skaergaard intrusion, except sample number IVN-14. The latter is from the marginal border group in Invarmuit island 36 m from the contact with the upper zone a of the layered series. The sample positions are indicated by *X*. The contour intervals are in meters. **b** A simplified east-west cross sectional view of the intrusive body adapted from McBirney (1993)

readers are referred to McBirney (1993). As we will see later, the cooling rates retrieved in this work apply to the temperature range $\sim$ 340–400° C, and thus are not affected by the initial quenching effect suffered by the intrusive body near the contact with the surrounding rock.

Cation ordering kinetics and cooling rates of orthopyroxenes

In orthopyroxene, Fe^{2+} and Mg fractionate between two nonequivalent octahedral sites, M1 and M2. The preferred site of Fe^{2+} is M2 and that of Mg is M1, which is smaller of the two octahedral sites. The fractionation, which was first discovered by Ghose (1960), is fairly sensitive to temperature and thus serves as a recorder of the cooling rate of the host rock. The kinetic theory of the order-disorder process was developed by Mueller (1967, 1969), who treated it in terms of a homogeneous chemical exchange reaction, *viz*.,

$$Fe^{2+}(M2) + Mg(M1) \rightleftarrows Fe^{2+}(M1) + Mg(M2), \quad \text{(a)}$$

and developed an expression which relates the time scale for *isothermal* ordering to the ordering state through the disordering rate constant (K^+) and intracrystalline Fe–Mg distribution coefficient. In keeping with our earlier works (e.g., Ganguly et al. 1994; Ganguly and Tazzoli 1994), we designate the latter by k_D to distinguish it from the commonly used symbol K_D for intercrystalline distribution coefficient. For the exchange reaction (a), the intracrystalline distribution coefficient is explicitly defined as

$$k_D = \frac{(X_{Fe^{2+}}/X_{Mg})^{M1}}{(X_{Fe^{2+}}/X_{Mg})^{M2}}, \quad (1)$$

where X_i stands for mole fraction of the specified ion. A thorough exposition of Mueller's theory and a method of its application to cooling rate calculation of natural minerals on the basis of their quenched ordering states can be found in Ganguly (1982) and Ganguly et al. (1994). The method involves assumption of a continuous cooling model, calculation of the evolution of the ordering state in a crystal from an initial temperature in a series of isothermal steps approximating an assumed T–t relation, and varying the latter until a satisfactory match is obtained between the quenched ordering state in the numerical simulation and that in the natural crystal. The results are quite insensitive to errors in the determination of the initial temperature as long as it is within the temperature domain at which thermodynamic equilibrium is maintained, but are very sensitive to errors of the site occupancy data of the natural crystal, especially for those with low Fe concentration (Ganguly et al. 1989).

Salje and Kroll (1991) have discussed the application of Landau theory to the analysis of the order-disorder kinetics of minerals, and have shown that the Mueller theory closely corresponds to the Landau theory if the Gibbs free energy expansion as a function of order parameter in the latter theory is truncated after the quadratic term. Further, Schelnz (personal communication) has shown that the order-disorder kinetic data for orthopyroxene can be treated very well by the quadratic approximation of the Landau theory. In this work we would, thus, use the Mueller-Ganguly approach to calculate the cooling rates of orthopyroxenes from the Skaergaard gabbroic intrusion.

Site occupancy of orthopyroxene crystals

Separation, selection and analyses of orthopyroxene crystals

Separation of orthopyroxene crystals suitable for crystallographic studies turned out to be a very difficult task as most of the crystals that appeared as orthopyroxene under a binocular microscope turned out to be either olivine or clinopyroxene in the single crystal X-ray diffraction pattern. After a laborious search, seven orthopyroxene crystals were selected from the five rock samples mentioned above, of which two were from the lower zone b sample SK90-5. These crystals were optically homogeneous, free of inclusions, and had dimensions ranging between $0.17 \times 0.17 \times 0.17$ and $0.23 \times 0.26 \times 0.50$ mm. After collection of X-ray data, the crystals were analyzed in an electron microprobe (Cameca Superprobe) to determine their bulk compositions, which were used as constraints to calculate the site populations. Unfortunately, in the process of transferring the crystals from the X-ray mounts to microprobe mounts, two crystals, one from IVN-14 and the other from SK90-5, were lost.

Although none of the crystals showed any exsolution feature either in X-ray maps of Ca distribution, or under an optical microscope, optical examination of thin sections of the rock samples revealed all orthopyroxenes to be inverted pigeonites with exsolution lamellae of augite. However, the distribution of the exsolved lamellae was nonuniform within large orthopyroxene (inverted pigeonite) grains, some of which had small domains free of optically visible exsolution near the grain boundaries. These domains are of comparable size to the crystals used in the X-ray structure refinement. It, therefore, seems possible that the crystals selected for X-ray structure refinement represent optically homogeneous fragments of larger crystals of inverted pigeonites. The failure to detect any exsolution-free orthopyroxene under the optical microscope prompted us to re-examine the single crystal X-ray data used in the selection of the samples. Very careful analyses of the X-ray data showed extremely weak (*Okl*) reflections with $k = 2n + 1$, which should be extinct in the *Pbca* space group, and can be ascribed to the presence of exsolved clinopyroxene (Domeneghetti et al. 1995a). Thus, the orthopyroxene crystals selected for site occupancy study should be considered as inverted pigeonites with very small amounts of submicroscopic exsolution of augites. Based on the intensity of the (*Okl*) reflections, we believe that the amount of exsolved augites in an orthopyroxene (inverted pigeonite) is $\leq 2\%$.

To ensure the accuracy of the site occupancy data required for cooling rate calculations (Ganguly et al. 1989), the bulk compositions of the crystals also had to be determined with very high degree of accuracy. Thus, all microprobe analyses were performed against *synthetic* end-member mineral standards, which were also used by Ganguly et al. (1994), and the composition at each spot was determined by counting for 100 s at the peak and 100 s at the background, using 15 kV accelerating voltage and 25 nA beam current. No systematic compositional variation was found in any crystal. Except for the orthopyroxene crystal from the rock sample SK90-5, the bulk composition of each crystal represents the average of between 12 and 15 spot analyses in which the oxide total was 100 $\pm$ 1; for SK-90–5, the bulk composition represents the average of 59 such analyses. Following Ganguly et al. (1994), each average composition was adjusted within one standard deviation (1σ) limit of the mean to satisfy the absolute crystal chemical constraints on the occupancy of the tetrahedral (T) and octahedral (M) sites (2.000 atoms per site for six oxygens in a formula unit) and charge neutrality of the bulk crystal (12.000 positive charge). The above constraints also ensure that there is no significant difference between the charge deficiency of the T-site (due to substitution for Si) and the charge excess in the M-site (due to substitution for 2 + ions).

Wet chemical analyses of orthopyroxenes from the lower zone of the Skaergaard intrusion show that $\sim 5\%$ of total iron is present as Fe^{3+} (Brown and Brown 1957). However, the above crystal chemical constraints cannot be satisfied with any significant amount of Fe^{3+} in the orthopyroxene crystals selected for X-ray study. The maximum amount of Fe^{3+} that can be accommodated is 0.0014 per six oxygens in the formula unit (or $\sim$ 0.2% of total iron) of sample CG-372. We have, thus, assumed all iron to be ferrous in the site occupancy refinement of the crystals (it is possible that the ferric iron determined by the wet chemical analyses of orthopyroxene separates was derived from oxide inclusions). The initial and adjusted bulk compositions of the crystals are summarized in Table 1. The potential effect of the permissible small concentration of ferric iron on the site occupancy data of sample CG-372 and on the consequent cooling rate calculations is discussed in later sections. Since there are (optically invisible) augite exsolutions in the orthopyroxenes, the analyzed bulk composition of a grain must be somewhat different from the true bulk composition of the host orthopyroxene. However, this difference should be negligible as the intensity of clinopyroxene reflections indicates extremely small amounts ($\leq 2\%$) of augite exsolutions.

X-ray data collection

Single crystal X-ray intensity data were obtained using a Phillips PW 1100 four-circle automated diffractometer and monochromatic (graphite monochromater) MoK_α radiation ($\lambda = 0.71073$ Å). The cell parameters of the orthopyroxene crystals and other data pertaining to structure refinement are summarized in Table 2. The cell parameters were determined using an improved version of Cannillo et al. (1983) of the Phillips LAT routine. Net X-ray intensities were determined by measuring step scan profiles and analyzing them by the Lehmann and Larsen (1974) $\sigma(I)/I$ method as modified by Blessing et al. (1974). The equivalent reflections hkl and $\bar{h}kl$ were measured using the ω scan mode within the θ ranges summarized in Table 2. The intensities were corrected for absorption using the semi-empirical method of North et al. (1968) and the values for the equivalent reflections were averaged. Only reflections with intensity $I > 3\sigma(I)$, were considered as observed in the structure refinement and given equal weight. This scheme of weighting and selection of reflections is the same as that followed by Molin et al. (1991) and Yang and Ghose (1994) for the calibration of site occupancies of orthopyroxene crystals as a function of temperature, which have been used in the calculation of cooling rates in this work. As discussed by Ganguly et al. (1994), the same procedure should be followed in the calibration of site occupancy as a function of temperature and in the determination of the site occupancies of the pyroxene crystals of interest in the cooling rate calculations, so that any inherent error in the procedure of weighting reflections etc. become self-cancelling.

The structure refinements were done in the space group *Pbca* without chemical constraints using an improved version of the least squares program ORFLS (Busing et al. 1962). The program assigns two scattering curves f_1 and f_2 to each site, and refines the site occupancy factors x(f) with the constraint that $x(f_1) + x(f_2) = 1$. The mean atomic number (m.a.n.) for a site (Table 2) is given by $x(f_1)N_1 + x(f_2)N_2$, where N_1 and N_2 are the number of electrons corresponding to the scattering curves f_1 and f_2. The atomic scattering curves are taken from the International Tables of X-ray Crystallography (1974) and from Tokonami (1965). The ionization states used were 2^+ for Si, Mg and Fe, and 1.5^- for O. In addition to scale factor and extinction coefficient, 30 atomic positional and anisotropic displacement parameters were refined, varying all parameters simultaneously. No correlation greater than 0.65 was observed. The final difference-Fourier maps were featureless, and the conventional agreement indices or R factors, as summarized in Table 2, varied between 1.6 and 2.6%. The final atomic parameters and the observed and calculated structure factors are available from the authors.

Table 1 Initial (I) and adjusted (A) bulk compositions of orthopyroxene crystals from the Skaergaard Intrusion. Each initial bulk composition represents the average of the indicated number of spot analyses on a single crystal

	IVN-14 (I)	Sigma[a]	IVN-14 (A)	CG-379 (I)	Sigma	CG-379 (A)	CG-372 (I)	Sigma	CG-372 (A)
# Analyses	13			15			14		
Si	1.9770	0.0080	1.9720	1.9670	0.0040	1.9660	1.9640	0.0080	1.9680
Al	0.0320	0.0070	0.0360	0.0420	0.0010	0.0410	0.0390	0.0010	0.0396
Ti	0.0099	0.0003	0.0099	0.0135	0.0005	0.0135	0.0121	0.0004	0.0121
Cr	0.0010	0.0010	0.0010	0.0000		0.0000	0.0000		0.0000
Mg	1.1990	0.0100	1.1997	1.2300	0.0060	1.2307	1.2110	0.0090	1.2095
Fe	0.6980	0.0070	0.6985	0.6580	0.0030	0.6591	0.6850	0.0060	0.6834
Mn	0.0150	0.0010	0.0153	0.0135	0.0010	0.0142	0.0140	0.0010	0.0130
Ni	0.0010	0.0010	0.0014	0.0010	0.0010	0.0017	0.0013	0.0006	0.0010
Ca	0.0650	0.0010	0.0653	0.0730	0.0050	0.0738	0.0750	0.0030	0.0735
Na	0.0010	0.0010	0.0010	0.0000		0.0000	0.0000		0.0000
Total	3.9989		4.0001	3.9980		4.0000	4.0014		4.0001
Charge	12.0036		11.9999	11.9990		12.0000	11.9940		11.9999
Al(T)[b]	0.0230		0.0280	0.0330		0.0340	0.0360		0.0320
Al(M)[b]	0.0090		0.0080	0.0090		0.0070	0.0030		0.0075
d(chr(M))[c]	0.0288		0.0278	0.0360		0.0340	0.0272		0.3170
d(M-T)[d]	0.0058		-0.0002	0.0030		0.0000	− 0.0088		− 0.0003
M-cations	1.9989		2.0001	1.9980		2.0000	2.0014		2.0001
T-cations	2.0000		2.0000	2.0000		2.0000	2.0000		2.0000

[a] Sigma: standard deviation from the mean of the spot analyses
[b] Al(T): Al in T site; Al(M): Al in M site
[c] d(chr(M)): excess positive charge in M site due to the substitution for 2 + cations
[d] d(M-T): difference between the charge excess in M site and the charge deficiency in T site

Table 2 Cell parameters and other data on structure refinement of orthopryoxene crystals from the Skaergaard intrusion. The standard deviations are in parentheses. R_{obs} is the conventional agreement index, whereas I_{obs} is the number of nonequivalent reflections with $I > 3\sigma(I)$ *that were used in the structure refinements*; *m.a.n. is the mean atomic number*

	a (Å)	*b* (Å)	*c* (Å)	*V* (Å^3)	θ Range	R_{obs}	N. of I_{obs}	m.a.n. (M1)	m.a.n. (M2)
IVN-14	18.312 (6)	8.892(2)	5.220(2)	850.0	2–60°	1.64%	1456	12.82(6)	21.73(6)
SK379	18.308(9)	8.887(3)	5.218(2)	849.0	2–30°	1.90%	984	12.85(9)	20.94(9)
SK380	18.315(9)	8.900(3)	5.220(2)	850.1	2–30°	2.21%	942	13.02(9)	22.04(12)
CG-372	18.310(6)	8.889(3)	5.218(2)	849.3	2–45°	2.56%	2144	12.87(6)	20.98(9)
CG-372	18.311(12)	8.892(6)	5.219(3)	849.8	2–40°	2.17%	1812	12.94(6)	21.38(7)
SK90-5	18.319(4)	8.899(2)	5.221(1)	851.2	2–40°	1.92%	1250	13.03(6)	22.09(6)
SK90-5	18.319(6)	8.899(2)	5.218(2)	850.7	2–40°	2.36%	1315	13.02(9)	21.85(9)

Site occupancy determination

The site occupancies were calculated using the results of structure refinements and bulk compositional data for the individual crystals, as determined by average of microprobe spot analyses and crystal chemical constraints (Table 1). The best value of the atomic fraction of an element in a given site was determined through a minmization procedure using the program MINUIT of James and Ross (1975). The quantity minimized was $\Sigma[(Q_{obs} - Q_{calc})/\sigma(Q_{obs})]^2$, that is the sum of the squares of the residuals between the observed and calculated values of the chemical and structural parameters (Q), weighted inversely by their respective standard deviations (σ). The chemical parameters are the atomic fractions of the elements (Si, Al, Ti, Cr, Mg, Fe, Mn, Ni, Ca and Na), as determined by microprobe analyses, whereas the structural parameters are the mean atomic numbers (m.a.n.) at the M1 and M2 sites, and the mean SiB-O and M1-O bond distances. The calculated value of the last distance is corrected by an empirical factor to account for the influence of the M2 site on the size of the M1 polyhedron (Domeneghetti et al. 1995b). It was assumed, as is the common practice (e.g., Domeneghetti et al. 1985; Tazzoli and Domeneghetti 1987; Yang and Ghose 1994, Molin 1989), that ^{VI}Al, Cr^{3+} and Ti are confined to the M1 site, Ca and Na to the M2 site, and that Mn and Ni partitioned between the two octahedral sites in the same way as Fe^{2+} (Hawthorne and Ito 1978) and Mg, respectively. The structural sites were considered fully occupied and the overall charge balance of the crystals for the substitutions of $^{VI}(Fe^{2+}, Mg)$ and ^{IV}Si was ensured by the constraint $X^{AlAl} + X^{Fe^{3+}} + X^{Cr} = X^{Na} + X^{IVAl}$, where X denotes the atomic fraction in a specific site. The results of the site occupancy determination are summarized in Table 3, and selected interatomic distances are given in the Appendix.

Ferric iron, if present, would be strongly partitioned into the M1 site (e.g., Molin et al 1991). If we now insert all the ferric iron (0.0014 atoms for six oxygens in a formula unit) that could be accommodated in the crystal CG-372 into its M1 site, then the Fe^{2+} content of this site will decrease by 0.0014. However, this maximum limiting change is significantly less than the uncertainty (0.003) of the site occupancy data. The other crystals can accomodate much less Fe^{3+}.

CG-380 (I)	Sigma	CG-380 (A)	SK90-5 (I)	Sigma	SK90-5 (A)
12			59		
1.9710	0.0030	1.9700	1.9767	0.0050	1.9716
0.0355	0.0005	0.0350	0.0351	0.0060	0.0320
0.0120	0.0004	0.0123	0.0124	0.0006	0.0124
0.0004	0.0001	0.0004	0.0002	0.0004	0.0002
1.1500	0.0030	1.1505	1.1666	0.0184	1.1716
0.7400	0.0050	0.7404	0.7141	0.0195	0.7191
0.0145	0.0013	0.0149	0.0148	0.0009	0.0157
0.0012	0.0005	0.0016	0.0010	0.0008	0.0018
0.0745	0.0023	0.0749	0.0706	0.0155	0.0756
0.0000	0.0000	0.0000	0.0000	0.0000	0.0000
3.9991		4.0000	3.9915		4.0000
12.0001		12.0001	11.9965		12.0001
0.0290		0.0300	0.0233		0.0284
0.0065		0.0050	0.0118		0.0036
0.0309		0.0300	0.0368		0.0286
0.0019		− 0.0000	0.0135		0.0002
1.9991		2.0000	1.9915		2.0000
2.0000		2.0000	2.0000		2.0000

Thus, the assumption that all iron is in the ferrous state does not introduce any significant error into the intracrystalline distribution coefficient, k_D, for the selected crystals.

Kinetic and thermodynamic data

Calculation of the cooling rates on the basis of the quenched cation ordering states requires data on either the cation ordering or the disordering kinetics as a function of temperature, composition and f_{O_2}, and of equilibrium intracrystalline fractionation (k_D) as a function of temperature and composition. Ganguly and Tazzoli (1994) analyzed the available data on the disordering kinetics of orthopyroxene which are at f_{O_2} conditions between those defined by the WI buffer and 0.8 log units above the WI buffer (Besancon 1981; Anovitz et al. 1988), and developed an optimized expression for the disordering rate constant as a function of temperature and X_{Fe}. Their expression, which is used in the present work, is as follows.

$$\ln K^{+} = (26.2 + 6.0 X_{Fe}) - \frac{31{,}589}{T},\ \mathrm{min}^{-1} \quad (2)$$

No experimental data are available to assess the f_{O_2} dependence of the rate constant, but the latter is expected to increase with increasing f_{O_2} as $\sim f_{O_2}^{1/6}$ on the basis of the expected dependence of point defect concentration on f_{O_2} through homogeneous redox equilibrium of ferrous and ferric iron (Buening and Buseck 1973; Morioka and Nagasawa 1991; Chakraborty and Ganguly 1991). The f_{O_2} conditions of the Skaergaard samples, all of which were collected from the lower zone, at temperatures near the closure temperature of cation ordering ($\sim$ 340–400° C, see Table 3) are not known, but one can make a reasonable estimate of f_{O_2} from the suggestion of Sato and Valenza (1980) that the f_{O_2} of the lower and middle zone rocks was controlled by graphite. This suggestion was based on the observation that the lower and middle zone samples undergo irreversible self-reduction when heated to temperatures above 1200° C, which is a behavior similar to that observed in natural and synthetic samples containing graphite. Sato and Valenza (1980) quoted estimates of pressure of the lower zone which varied between 1.2 and 2 kbar. Taylor and Forester (1979) and Norton and Taylor (1979) demonstrated pervasive interaction of H_2O, derived from the country rock, with the Skaergaard pluton as it crystallized and cooled. We, thus, assume that the f_{O_2} condition of the lower zone

Table 3 Summary of the site occupancy data, closure temperatures of ordering (T_C) and cooling rates of orthopyroxene crystals from Skaergaard Intrusion. The 1 σ uncertainty of the site occupancy data, shown as parenthetical values (right justified), introduces uncertainty of a factor of $\sim$ 2 in the values of the time constant η and cooling rates. Fe and Mn have been grouped together in the calculation of K_D

Sample No.	IVN-14	CG-379	CG-380	CG-372	SK90-5
M1 Site:					
Mg	0.929(2)	0.917(30)	0.914(3)	0.919(2)	0.919(3)
Fe	0.050(2)	0.060(3)	0.066(3)	0.059(2)	0.063(3)
Cr^{3+}	0.001	—	0.000	—	0.000
Al	0.008	0.007	0.005	0.008	0.003
Ti^{4+}	0.010	0.013	0.012	0.012	0.012
Mn	0.001	0.001	0.001	0.001	0.001
Ni	0.001	0.001	0.001	0.001	0.001
M2 Site:					
Mg	0.274(2)	0.318(3)	0.237(4)	0.294(2)	0.261(3)
Fe	0.646(2)	0.597(3)	0.673(4)	0.621(2)	0.649(3)
Mn	0.014	0.013	0.014	0.012	0.014
Ca	0.065	0.072	0.075	0.073	0.075
Na	0.001	—	—	—	—
Ni	0.000	0.001	0.000	0.000	0.000
k_D	0.023	0.035	0.025	0.030	0.027
T_C (°C)	337	402	353	379	364
$\eta(K^{-1}year^{-1}) \times 10^{-8}$	0.2	45	0.8	6.5	1.4
CR @ T_C (K/ka)	1	273	3	28	6

rocks was controlled by C(graphite)-vapor equilibrium at 1–2 kbar pressure. Restricting the fluid species to H_2O, CO_2, CO, CH_4 and H_2, but with the constraint that H/O ratio is 2/1 (i.e., H_2O is the only source of H and O, and there is no preferential loss of either species), we obtain $f_{O_2} \approx 10^{-27}$ bar at 2 kbar, 700 K for the graphite-vapor equilibrium, as compared to $f_{O_2} = 10^{-32.8}$ bar defined by WI buffer at the same P–T condition. The f_{O_2} for the graphite-vapor equilibrium was calculated using the fluid properties of Belonoshko and Saxena (1992), whereas that for WI buffer was derived from thermochemical data summarized by Robie et al. (1978). The calculated f_{O_2} value for the graphite-vapor equilibrium is in excellent agreement with experimental results of Ulmer and Luth (1991) for f_{O_2} defined by graphite-COH fluid as a function of P and T. Assuming that it varies as $(f_{O_2})^{1/6}$, the disordering rate constant given by Eq. 2 would then be enhanced by a factor of ~ 8 by the change of f_{O_2} from values between the WI and 0.8 log f_{O_2} unit above WI to C(graphite)-H-O equilibrium.

Molin et al. (1991) determined the temperature dependence of the equilibrium Fe^{2+}–Mg fractionation between the M1 and M2 sites of an orthopyroxene crystal from Johnstown meteorite. An average of 55 spot analyses for which the oxide sum equalled 100 ± 1 yields the composition (Molin, personal communication): $(Fe_{.458}Mg_{1.437}Cr_{.024}Mn_{.014}Ti_{.003}Ca_{.054}\ Al_{.009}\ Na_{.001})^{VI}(Si_{1.963}Al_{.037})^{IV}O_6$. Molin et al.'s calibration was based on single crystal X-ray determination of site occupancies of the quenched orthopyroxene crystal after annealing at several temperatures between 700 and 1100° C. At each temperature, the equilibrium ordering state was very tightly constrained by 'reversal' experiments, i.e. approaching from initial states which were more ordered and more disordered than the expected equilibrium state. Molin (personal communication) has modified the initial calibration using the more refined bulk compositional constraint, quoted above, and treating Fe + Mn as a single component (as in this work). The refined calibration is in almost exact agreement with the results of Yang and Ghose (1994) at $727 - 927°$ C using a synthetic orthopyroxene crystal with $Fe^{2+}/(Fe^{2+} + Mg)$ ratio similar to that in the Johnstown sample. The latter workers determined the site occupancies by in-situ high temperature X-ray diffraction studies. Least squares fit of the two datasets yields

$$ln k_D = -\frac{2739.5}{T} + 0.7048 \quad (r^2 = 0.998) \tag{3}$$

The excellent agreement between the data of Molin and Yang and Ghose for orthopyroxene crystals with similar Fe/(Fe + Mg) ratios (0.23–0.25) suggests that the net effects of the small amount of non-binary components in the Johnstown sample on the intracrystalline Fe–Mg fractionation is negligible. The concentrations of these components in the Skaergaard samples

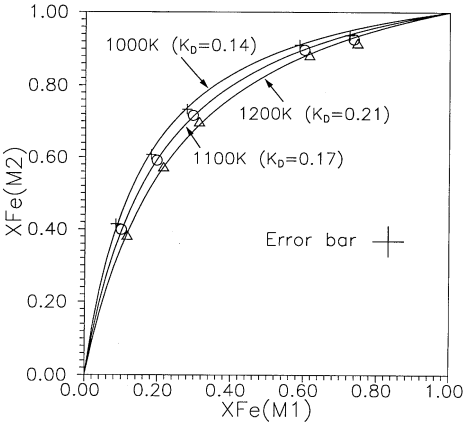

Fig. 2 Fractionation of Fe^{2+} between the M1 and M2 sites of orthopyroxenes, as determined by Yang and Ghose (1994) for synthetic samples in the Fe–Mg join by in situ high temperature X-ray diffraction, and comparison of the data with the fractionations calculated on the basis of constant k_D value at each temperature

are similar to that in the Johnstown sample. However, since the Skaergaard samples have significantly higher concentration of Fe (Fs_{35-39}) relative to that in the Johnstown sample (Fs_{23}), it is important to evaluate the effect of Fe/Mg ratio on the intracrystalline Fe/Mg fractionation. Yang and Ghose (1994) determined this effect from in-situ high temperature X-ray diffraction data of synthetic Fe-Mg orthopyroxene crystals with Fs content between 25 and 83 mol%. Their data are illustrated in Fig. 2 in terms of what is often referred as a Rozeboom plot. We have fitted these data according to constant k_D value at each temperature. It is evident that except for the data with the highest concentration of Fe, i.e. Fs = 83%, all isothermal data conform to a constant k_D value. The misfits of the calculated distribution isotherms to the data for crystals with Fs_{83} are also well within the uncertainties of the data. However, regardless of whether these misfits are real or not, it is safe to conclude that there is no significant effect of Fe/Mg ratio on k_D within at least the compositional range Fs_{25}–Fs_{75}.

Cooling rates of the orthopyroxene crystals and implications

We have modeled the cooling rates using an asymptotic cooling law, $1/T = 1/T_0 + \eta t$, where T_0 is the initial temperature and η is a time constant (K^{-1} year^{-1}). The η values required to produce quenched ordering states in the simulated evolution of ordering vs temperature exactly matching (within three decimal places) those in the respective orthopyroxene crystals are summarized in Table 3. These calculations were carried out using the $\ln k_D$ vs T relation given by Eq. 3 and the modified value of the disordering rate constant discussed above (i.e. 8 times that given by eqn. (2) to correct for the f_{O_2} effect). Also listed in Table 3 are the

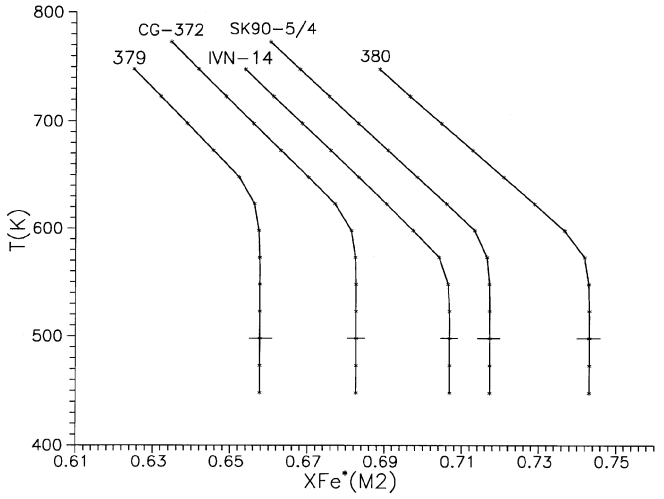

Fig. 3 Simulated evolutions of the site occupancy of Fe + Mn, denoted collectively as Fe*, in the M2 site of orthopyroxene crystals from the Skaergaard intrusion as a function of temperature. The *horizontal bars* represent the observed M2 site occupancy of Fe* of the samples as determined by single crystal X-ray diffraction (Table 3). The value of the cooling time constant (η) for each sample corresponding to the simulated evolution of its site occupancy is summarized in Table 3

closure temperatures (T_c) corresponding to the quenched Fe–Mg ordering states of the samples (337–402° C), as calculated from Eq. 3, and the cooling rates (given by $-\eta T^2$) at the T_c for each sample. The experimental $\ln k_D$ vs $1/T$ calibration has been linearly extrapolated to the T_c values. Such linear extrapolation is justified since the ΔC_p of the intracrystalline Fe–Mg exchange reaction must be extremely small (Ganguly et al. 1994).

The simulated evolution of the ordering states of the samples is illustrated in Fig. 3. Each evolutionary path of the ordering state has three segments: a high temperature segment in which the ordering state maintains equilibrium with temperature, a low temperature segment in which the ordering state remains essentially fixed, and a small intermediate temperature segment defining the transition from thermodynamic equilibrium to quenching. The fact that an orthopyroxene crystal is an inverted pigeonite has no perceptible effect on its quenched ordering state corresponding to a cooling time constant, η, since the inversion took place within the temperature regime within which the ordering state maintained equilibrium with temperature. The cooling rates strictly hold only at temperatures near T_C, where they are also fairly insensitive to the nature of the cooling models (Ganguly et al. 1994).

In their work on the redistribution of mass, energy and momentum during the crystallization of the Skaergaard pluton, Norton and Taylor (1979) calculated the transport of relatively low $\delta^{18}O$ fluids from basalt country rocks into the pluton. Satisfactory match between the measured (Taylor and Forester 1979) and simulated shifts of the $\delta^{18}O$ values was obtained by assuming bulk rock permeability values of 10^{-12} (model S1) and 10^{-13} cm^2 (model S2) for the intrusive body, and 10^{-11} cm^2 and 10^{-16} cm^2 for the surrounding basalt and gneiss, respectively. Fig. 4 is a reproduction from Norton and Taylor (1979) showing the thermal evolution of two hypothetical samples at two posi-

Fig. 4 Numerical model of the cooling histories of two hypothetical samples from each of the three levels, upper border group (UBG: left panel), sandwich horizon (SH: middle panel) and the middle zone (MZ: right panel) of the Skaergaard intrusion, as calculated by Norton and Taylor (1979). The sample locations in each level are indicated by *numbered triangles* within schematic cross section of the pluton. The assumed permeabilities for the pluton are 10^{-12} cm^2 for the model S1 (upper set) and 10^{-13} cm^2 for the model S2 (lower set). In both models, the surrounding basalt and gneiss are assumed to have permeabilities of 10^{-11} cm^2 and 10^{-16} cm^2, respectively. The *dashed lines* illustrate the cooling rates at selected temperatures

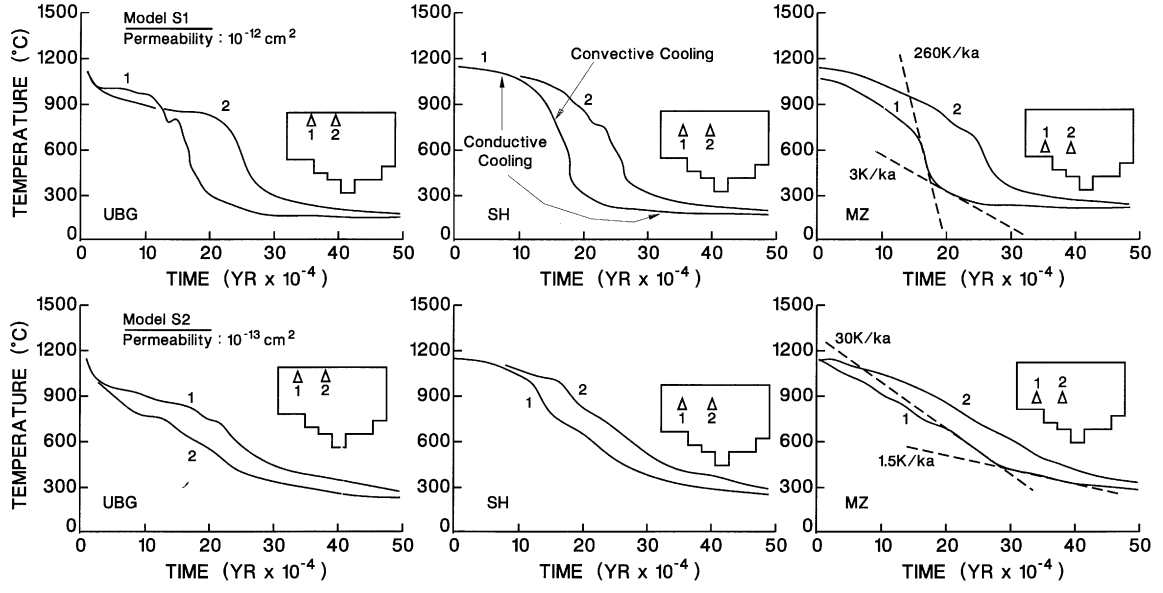

tions from each of the following zones: the upper border group (UBG), sandwich horizon (SH) and the middle zone (MZ). The locations of the samples are marked by numbered (1 and 2) triangles within a schematic cross section of the pluton, which is shown within each sub-figure. Thermal evolutions were calculated for both models S1 and S2. Each thermal model has three characteristic segments, marked by relatively slow conductive cooling at high and low temperatures and relatively fast convective cooling at intermediate temperatures. The latter is a consequence of fluid circulation, and its high temperature limit marks the opening of fractures in the solidified pluton, whereas the low temperature limit marks the decrease in the buoyancy force of water (following long period of circulation) to the point where conduction dominated again.

Regardless of the level in the pluton, the simulated cooling rates of the samples are essentially the same around the T_Cs of cation ordering of the orthopyroxene samples ($\sim$ 340–400° C), which mark the approximate transition from convective to conductive cooling. Thus, although Norton and Taylor (1979) did not present a thermal model for the lower zone b rock and the marginal border group, it is reasonable to assume that the cooling rates around the T_C of cation ordering are similar to those in the other levels or segments. Except for sample CG-379, the cooling rates of the orthopyroxene samples range from 1 to 28° C/ka at $T_C \sim$ 340–380° C (with an uncertainty of a factor of ~ 2 arising from the standard deviation of the site occupancy data), which agree well with the cooling rates that are implied by the thermal models S1 and S2 of Norton and Taylor (1979). However, the calculated cooling rate of the sample CG-379, which is $\sim$ 270° C/ka at $T_C \approx$ 400° C, is too high for the cooling rates permissible by the model S2, but agrees well with the convective cooling rate in the model S1. Thus we conclude that although both models S1 and S2 yield shifts of $\delta^{18}O$ values which are compatible with those observed in the Skaergaard pluton, the model S1, and hence an average permeability value of 10^{-12} cm^2 for the pluton is probably more appropriate.

Although all orthopyroxene crystals went through the convective thermal domain, the difference among the cooling rates reflected by their quenched ordering states can be explained by subtle differences among the temperatures at which each experienced the transition from the convective to conductive cooling. For example, the relatively rapid cooling rate in the convective domain in the model S1 yields T_C of cation ordering in orthopyroxene of $\sim$ 400° C. Thus, if the transition from convective to conductive cooling took place below this temperature, orthopyroxene would reflect the convective cooling rate. On the other hand, if the transition took place at a higher temperature, the cation ordering state in the orthopyroxene would reflect a slower cooling rate.

Appendix

Selected interatomic distances (Å) of the orthopyroxene samples from the Skaergaard intrusion. The standard deviations (right justified) are in parentheses

	IVN-14	SK379	SK380	CG-372/1	CG-372/5	SK90-5/1	SK90-5/4
SiA-O1A	1.610(1)	1.611(1)	1.610(1)	1.613(1)	1.611(1)	1.612(1)	1.611(1)
SiA-O2A	1.596(1)	1.595(1)	1.597(2)	1.598(1)	1.596(1)	1.596(1)	1.595(1)
SiA-O3A	1.639(1)	1.639(1)	1.637(2)	1.639(1)	1.643(1)	1.637(1)	1.639(1)
SiA-O3A	1.658(1)	1.658(1)	1.659(2)	1.659(1)	1.656(1)	1.661(1)	1.660(1)
⟨SiA-O⟩	1.626	1.626	1.626	1.627	1.626	1.626	1.626
SiB-O1B	1.621(1)	1.623(1)	1.624(1)	1.623(1)	1.621(1)	1.621(1)	1.622(1)
SiB-O2B	1.599(1)	1.599(1)	1.598(2)	1.599(1)	1.599(1)	1.598(1)	1.599(1)
SiB-O3B	1.673(1)	1.672(1)	1.670(2)	1.674(1)	1.673(1)	1.673(1)	1.668(1)
SiB-O3B	1.665(1)	1.668(1)	1.665(2)	1.667(1)	1.667(1)	1.666(1)	1.668(1)
⟨SiB-O⟩	1.640	1.640	1.639	1.640	1.640	1.639	1.640
M1-O1A	2.032(1)	2.033(1)	2.034(2)	2.034(1)	2.035(1)	2.034(1)	2.033(1)
M1-O1A	2.146(1)	2.148(1)	2.146(2)	2.146(1)	2.148(1)	2.148(1)	2.149(1)
M1-O1B	2.170(1)	2.171(1)	2.170(2)	2.171(1)	2.171(1)	2.172(1)	2.170(1)
M1-O1B	2.060(1)	2.061(1)	2.061(2)	2.061(1)	2.062(1)	2.062(1)	2.064(1)
M1-O2A	2.035(1)	2.031(1)	2.036(2)	2.029(1)	2.032(1)	2.032(1)	2.035(1)
M1-O2B	2.063(1)	2.060(1)	2.063(2)	2.063(1)	2.064(1)	2.066(1)	2.064(1)
⟨M1-O⟩	2.084	2.084	2.085	2.084	2.085	2.086	2.086
M2-O1A	2.161(1)	2.158(1)	2.165(2)	2.157(1)	2.158(1)	2.162(1)	2.163(1)
M2-O1B	2.119(1)	2.116(1)	2.120(2)	2.116(1)	2.117(1)	2.122(1)	2.120(1)
M2-O2A	2.061(1)	2.061(1)	2.059(2)	2.063(1)	2.061(1)	2.060(1)	2.059(1)
M2-O2B	2.006(1)	2.005(1)	2.009(1)	2.002(1)	2.002(1)	2.005(1)	2.006(1)
M2-O3A	2.367(1)	2.359(1)	2.367(2)	2.360(1)	2.361(1)	2.368(1)	2.363(1)
M2-O3B	2.515(1)	2.502(1)	2.516(2)	2.502(1)	2.506(1)	2.514(1)	2.512(1)
⟨M2-O⟩	2.205	2.200	2.206	2.200	2.201	2.205	2.204

Acknowledgements We are grateful to Professors Dennis Bird, Alexander McBirney, Stewart McCallum and Denis Norton for donations of the samples from the Skaergaard intrusion, and to Professor Norton for helpful discussions. Constructive reviews by Professors Eric Essene, Surendra Saxena and Tim Grove are gratefully acknowledged.This research was supported by an U.S. National Science Foundation grant EAR 9117927, NASA grant NAG 9–460 (J.G.) and financial support (C.D.) from the Italian Consiglio Nazionale delle Ricerche (CNR).

References

Anovitz LM, Essene EJ, Dunham WR (1988) Order-disorder experiments in orthopyroxene: implications for orthopyroxene geospeedometer. Am Mineral 73:1060–1073

Besancon JR (1981) Rate of cation ordering in orthopyroxenes. Am Mineral 66:965–973

Belonoshko AB, Saxena SK (1992) Equations of state of fluids at high temperature and pressure (water, carbon dioxide, methane, carbon monoxide, oxygen, and hydrogen). In: Saxena SK (ed) Thermodynamic data: systematics and estimation (Advances in Physical Geochemistry Vol 9). Springer, Berlin Heidelberg New York, pp 81–97

Blessing RH, Coppens P, Becker P (1974) Computer analysis of step-scanned X-ray data. J Appl Crystallogr 7:488–492

Brown GM, Brown PE (1957) Pyroxenes from the early and middle stages of fractionation of the Skaergaard intrusion, East Greenland. Mineral Mag 31:511–543

Buening DK, Buseck PR (1973) Fe-Mg lattice diffusion in olivine. J Geophys Res 8:6852–6862

Busing WR, Martin KO, Levy HS (1962) ORFLS, a Fortran crystallographic least squares program. US NTIS, ORNL-TM-305

Cannillo E, Germani G, Mazzi F (1983) New crystallographic software for Philips PW 1100 single crystal diffractometer. CNR Centro di Studio per la Cristallografia, Internal Report 2

Chakraborty S, Ganguly J (1991) Compositional zoning and cation diffusion in garnet. In: Ganguly J (ed) Diffusion, atomic ordering and mass transport (Advances in Physical Geochemistry Vol 8). Springer, Berlin Heidelberg New York, pp 120–175

Domeneghetti MC, Molin GM, Tazzoli V (1985) Crystal-chemical implications of the Mg^{2+}–Fe^{2+} distribution in orthopyroxenes. Am Mineral 69:987–995

Domeneghetti MC, Molin GM, Stimpfl M, Tribaudino M (1995a) Orthopyroxene from the Serra de Mage meteorite: structure refinement and estimation of *C*2/*c* pyroxene contributions to apparent *Pbca* diffraction violations. Am Mineral 80:923–929

Domeneghetti MC, Molin GM, Tazzoli V (1995b) A crystal-chemical model for *Pbca* orthopyroxenes. Am Mineral 80:253–267

Ganguly J (1982) Mg–Fe order-disorder in ferromagnesian silicates II. Thermodynamics, kinetics, and geological applications. In: Saxena SK (ed) Advances in physical geochemistry, Vol 2. Springer, Berlin Heidelberg New York, pp 58–99

Ganguly J, Tazzoli V (1994) Fe^{2+}–Mg interdiffusion in orthopyroxene: retrieval from the data on intracrystalline exchange reaction. Am Mineral 79:30–937

Ganguly J, Bose K, Ghose S (1989) Fe^{2+}–Mg ordering in orthopyroxenes and the cooling rates of meteorites. Proc 20th Lunar Planet Sci Conf :331–332

Ganguly J, Yang H, Ghose S (1994) Thermal history of mesosiderites: constraints from compositional zoning and Fe–Mg ordering in orthopyroxenes. Geochim Cosmochim Acta 58:2711–2723

Ghose S (1960) Fe–Mg ordering in ferromagnesian minerals. Prog with Abstr, Am Cryst Assoc, Washington Meeting, 19

Hawthorne FC, Ito J (1978) Refinement of the crystal structures of $(Mg_{0.776}Co_{0.224})SiO_3$. Acta Crystallogr B34:891–893

International Tables for X-ray Crystallography (1974) Kynoch Press, Birmingham, Great Britain

James F, Ross M (1975) MINUIT, a system for function minimisation and analysis of the parameter errors and correlations. CERN/DD, Internal Report 75/20, Computer Physics 10:343–347

Lehmann MS, Larson FK (1974) A method for location of the peaks in step-scan measured Bragg reflections. Acta Crystallogr A30:580–584

McBirney AR (1993) Igneous petrology. Jones and Bartlett. Boston London

Molin GM (1989) Crystal-chemical study of cation disordering in Al-rich and Al-poor orthopyroxenes from spinel lherzolite xenoliths. Am Mineral 74:593–598

Molin GM, Saxena SK, Brizi E (1991) Iron-magnesian order-disorder in orthopyroxene crystal from the Johnstown meteorite. Earth Planet Sci Lett 105:260–265

Morioka M, Nagasawa H (1991) Ionic diffusion in olivine. In: Ganguly J (ed) Diffusion, atomic ordering and mass transport, (Advances in Physical Geochemistry Vol 8). Springer, Berlin Heidelberg New York, pp 176–197

Mueller RF (1967) Models for order-disorder kinetics in certain quasibinary crystals of continuously variable composition. J Phys Chem Solids 28:2239–2243

Mueller RF (1969) Kinetics and thermodynamics of intracrystalline distribution. Mineral Soc Am Spec Pap 2:83–93

North ACT, Phillips DC, Mathews FS (1968) A semi-empirical method of absorption correction. Acta Crystallogr A24:351–359

Norton D, Taylor HP Jr (1979) Quantitative simulation of the hydrothermal systems of crystallizing magmas on the basis of transport theory and oxygen isotope data: an analysis of the Skaergaard Intrusion. J Petrol 20:421–486

Robie RA, Hemingway BS, Fisher JR (1978) Thermodynamic properties of minerals and related substances at 298.15 K and 1 bar (10^5 Pa) pressure and higher temperatures. US Geol Surv Bull 1452:1–456

Salje EH, Kroll H (1991) Kinetic rate laws derived from order parameter theory III: Al, Si ordering in sanidine. Phys Chem Mineral 17:563–568

Sato M, Valenza M (1980) Oxygen fugacities of the layered series of the Skaergaard intrusion, East Greenland. Am J Sci 280–A:134–158

Taylor HP, Forester RW (1979) An oxygen and hydrogen isotope study of the Skaergaard intrusion and its country rocks: a description of a 55-m.y. old fossil hydrothermal system. J Petrol 20:355–419

Tazzoli V, Domeneghetti MC (1987) Crystal-chemistry of natural and heated aluminous orthopyroxenes. Phys Chem Mineral 15:131–139

Tokonami M (1965) Atomic scattering factors for O^{2-}. Acta Crystallogr 19:486

Ulmer P, Luth RW (1991) The graphite-COH fluid equilibrium in P, T, fO_2 space. Contrib Mineral Petrol 106:265–272

Wager LR, Deer WA (1939) Geological investigations in East Greenland, pt III. The petrology of the Skaergaard intrusion, Kangerdlugssuaq, East Greenland, Medd Groen, 105:1–352

Wager LR, Brown GM (1968) Layered igneous rocks. Freeman, San Francisco

Yang H, Ghose S (1994) In-situ Fe–Mg order-disorder studies and thermodynamic properties of orthopyroxenes $(Fe, Mg)_2Si_2O_6$. Am Mineral 79:633–643